Applied Catalysis B: Environmental 156–157 (2014) 307–313

Contents lists available at ScienceDirect

Applied Catalysis B: Environmental

journal homepage: www.elsevier.com/locate/apcatb

Composite Bi_2O_3–TiO_2 catalysts for toluene photo-degradation: Ultraviolet and visible light performances

María Natividad Gómez-Cerezo[a,b], Mario J. Muñoz-Batista[a], David Tudela[b], Marcos Fernández-García[a,**], Anna Kubacka[a,*]

[a] Instituto de Catálisis y Petroleoquímica, CSIC, C/Marie Curie 2, 28049 Madrid, Spain
[b] Departamento de Química Inorgánica, Facultad de Ciencias, Universidad Autónoma de Madrid, Campus Cantoblanco, 28049 Madrid, Spain

ARTICLE INFO

Article history:
Received 2 January 2014
Received in revised form 6 March 2014
Accepted 11 March 2014
Available online 20 March 2014

Keywords:
Photo-catalysis
Mineralization
Sunlight
Titania
Bismuth

ABSTRACT

A series of Bi_2O_3–TiO_2 composite catalysts with variable quantities of bismuth was prepared by a single pot microemulsion procedure, calcined at 450 °C, and evaluated in the gas-phase degradation of toluene. Samples improve the reaction rate and quantum efficiency of the TiO_2 anatase reference material by a maximum factor ca. 2.2 and increase significantly the selectivity to the total oxidation product, CO_2, upon both UV and sunlight-type excitation. A complete bulk and surface structural and electronic characterization using X-ray diffraction (XRD), X-ray photoelectron (XPS), Raman, and UV–vis spectroscopies was carried out to interpret the catalytic results. The presence of bismuth enhances the optical response of the composite material to the visible region and modifies the morphology of the titania component. The study interprets the enhanced photoactivity of the composite materials with respect to both Ti anatase and the beta Bi_2O_3 single oxide reference systems as a compromise between two effects: the contact of anatase with a Bi oxide phase as well as the anatase morphology modification along the Bi–Ti series. Both effects influence the photo-chemical activity of the composite materials and provide the basis to explain the optimum performance achieved with a material containing a 5 wt.% of bismuth oxide.

1. Introduction

Heterogeneous photocatalysis is an Advanced Oxidation Process using nanocrystalline semiconductors applied to environmental abatement in both liquid and gas phases but also to synthesis of high added value products. The first application is by far the most broadly used and it is essentially based in the excellent performance and stability of titania, the most prominent photocatalytic material, for the mineralization of typical pollutants, including refractory or non-biodegradable molecules, under mild conditions, e.g. room temperature and atmospheric pressure and using oxygen (air) as oxidant agent [1–4]. Anatase is clearly the most active phase among titania polymorphs largely because it shows a correct balance between its surface chemistry-related properties and the adequate physical properties for efficient handling of light-triggered charge carriers, allowing them to be involved in chemical steps at the surface [4]. The quest of improving anatase photo-degradation properties was however pursued almost from the beginning of the photocatalytic field. Several strategies were tested, being most popular those related to the electronic modification of titania through cationic [1,2,4–8], anionic [1,2,4,9–11], and anionic–cationic [2,4,12–17] (co)-doping, or the use of additional, visible-light-sensitized phases in intimate contact with TiO_2. Such sensitizing phases may have semiconductor [2,4,18–25] or metallic [2,4,26–30] nature.

Bismuth oxide is another semiconductor frequently used in photocatatalysis, particularly from recent times. It has four main crystallographic polymorphs, monoclinic alpha, tetragonal beta, body-centered cubic gamma and face-centered cubic delta Bi_2O_3. All of them can present band gap energies in the visible region and thus correspond to materials with potential for profiting from clean energy sources such as the sun [31]. Alpha and gamma polymorphs are reasonably stable phases but beta seems the most active one as a nanostructured material. This appears to result from a combination of factors related to the gain in light absorption power produced by a lower band gap energy as well as a more efficient handling of charge carriers after light excitation [31–35]. The stability of the beta phase is however rather limited, particularly in

* Corresponding author. Tel.: +34 91 585 4939; fax: +34 91 585 4760.
** Corresponding author. Tel.: +34 91 5854775.
E-mail addresses: mfg@icp.csic.es (M. Fernández-García), ak@icp.csic.es (A. Kubacka).

http://dx.doi.org/10.1016/j.apcatb.2014.03.024
0926-3373/

reaction conditions. Under reaction the degradation of the phase by effect of the carbonatation of the oxide, generation of defects and/or its slow transformation into alpha Bi_2O_3, presumably by local thermal effects, are commonly observed. Such issues would thus limit the use of the beta phase for general application in the photo-degradation of pollutants.

A way to solve the situation is the stabilization of the beta phase by contact with another semiconductor such as ZnO, TiO_2 or others [2,4,36,37]. In the case of titania, a Bi–Ti composite system may have a two-fold aim as may allow, as mentioned previously, the stabilization of the beta Bi_2O_3 phase but also would provide a way to overcome some weaknesses of titania. In particular an ambitious task corresponds to delineate materials which allow a profitable use of a renewable source as the sun. In the Bi–Ti composite system, this typically implies the improvement of the capabilities of both oxide components and both under UV and visible light(s). Bi_2O_3–TiO_2 composite systems have been therefore tested in several photocatalytic reactions like the degradation of dyes [38–42], penta-chlorophenol [43–45], carbamazepine [46] or bisphenol-A in the presence (i.e. simultaneous reduction) of Cr [47]. In all cases, the composite material displayed improved performance with respect to the parent oxides while excited with light having characteristic wavenumber about 420 nm. Only in a single case (Ref. [39]) the composite oxide-oxide system was tested under UV–vis excitation and thus their performance in respect to solar light utilization fully analyzed. The correct balance between UV and visible light capabilities is obviously of importance in the context of the solar to chemical energy conversion field [2,4].

Here we have analyzed the interaction of Bi_2O_3 and TiO_2 both under UV and visible lights. A microemulsión preparation method [48] was used to control the morphological variables of both oxides as well as to enhance the interface contact between them. Maximum activity is reached using relatively small molar ratios of the Bi oxide. This complicates the analysis of the Bi-containing component but here we will use the pure Bi system to obtain information about the polymorphism behavior at the preparation conditions. The analysis of single Bi_2O_3 and TiO_2 reference and Bi–Ti composite systems has been carried out using a combination of techniques including X-ray diffraction, porosimetry as well as Raman, ultraviolet and X-ray photoelectron spectroscopies. The photocatalytic behavior of the materials was explored as a function of the Bi content of composite samples. We tested the elimination of toluene as it is a very demanding reaction and thus constitutes a tough chemical test to assess the potential of the TiO_2-based systems in the photo-elimination of organic pollutants [49,50]. The optimum of the photocatalytic behavior is observed for UV and, less markedly, for sunlight-type excitation for a sample containing a 5 wt.% of bismuth. The composite material would not only improve activity with respect to the titania reference but also selectivity toward the total oxidation pathway (e.g. CO_2). The characterization results indicate that the presence of bismuth, likely in a beta-type oxide phase, promotes the physico-chemical modification of the titania component and is in the origin of the favorable effect on titania photo-catalytic performance.

2. Experimental

2.1. Catalyst preparation

Materials were prepared using a single pot microemulsion preparation method using *n*-heptane (Scharlau) as organic media, Triton X-100 (Aldrich) as surfactant and hexanol (Aldrich) as cosurfactant. Ti isopropoxide (Aldrich) and Bi nitrate (Aldrich) were used as precursor of the inorganic materials. Water/(Ti + Bi) and water/surfactant molar ratios were, respectively, 110 and 18 for all samples [50]. In all composite samples and the Bi_2O_3 reference, Bi nitrate was introduced in the aqueous phase of a microemulsión in presence of nitric acid (pH ca. 2.5). After 30 min of agitation of the microemulsion, the corresponding quantity of sodium carbonate (to obtain a $Bi_2O_2CO_3$ phase – see Ref. [51] for details) was introduced from the aqueous phase of a similar microemulsión. For nanocomposite samples, after 5 min of contact, titanium tetraisopropoxide was introduced into the previously resulting microemulsion drop by drop from a mixture with isopropanol (2:3). The titania reference was obtained with the microemulsión procedure with a pH at the polar phase equal to the Bi-containing materials. The resulting mixture was stirred for 24 h, centrifuged, and the separated solid precursors rinsed with water and methanol and dried at 110 °C for 12 h. After drying, the solid precursors were subjected to a heating ramp (2 °C min^{-1}) up to 450 °C, maintaining this temperature for 2 h. Samples names are Ti and Bi for the titania and bismuth single oxide reference, and *x*BiTi for the composite ones where *x* is the weight percentage measured as Bi_2O_3.

2.2. Characterization details

The BET surface areas and average pore volume and sizes were measured by nitrogen physisorption (Micromeritics ASAP 2010). XRD profiles were obtained with a Seifert D-500 diffractometer using Ni-filtered Cu Kα radiation with a 0.02° step and fitted using the Von Dreele approach to the Le Bail method [52]; particle sizes and microstrain were measured with XRD using the Williamson–Hall formalism [53]. Temperature treatments were carried out in the presence of dry air, from 25 to 750 °C with a ramp of 5 °C min^{-1}. For each temperature of analysis, the system was hold for 15 min prior taking the XRD pattern. Ti:Bi composition was analyzed by using inductively coupled plasma and atomic absorption (ICP-AAS; Perkin-Elmer, Optima 3300 DV).

XPS data were recorded on $4 \times 4\,mm^2$ pellets, 0.5 mm thick, prepared by slightly pressing the powered materials which were outgassed in the prechamber of the instrument at room temperature up to a pressure $<2 \times 10^{-8}$ Torr remove chemisorbed water from their surfaces. The SPECS spectrometer main chamber, working at a pressure $<10^{-9}$ Torr, was equipped with a PHOIBOS 150 multichannel hemispherical electron analyser with a dual X-ray source working with Ag Kα ($h\nu$ = 1486.2 eV) at 120 W, 20 mA using C *1s* as energy reference (284.6 eV). Surface chemical compositions were estimated from XP-spectra, by calculating the integral of each peak after subtraction of the "S-shaped" Shirley-type background using the appropriate experimental sensitivity factors and the CASA-XPS (version 2.3.15) software.

UV–vis transmission or diffuse reflectance spectroscopy experiments were performed with a Shimadzu UV2100 apparatus with a nominal resolution of ca. 1 nm using, for diffuse experiments, $BaSO_4$ as reference. Band gap values of the samples were obtained using the equation $\alpha h\nu = A(h\nu - Eg)^{n/2}$ (where α, h, ν, Eg, and A are absorption coefficient, Planck constant, radiation frequency, band gap and a constant, respectively), assuming an indirect band gap semiconductor behavior (n = 4). Band gap typical error is 0.03 eV [54].

2.3. Photo-catalytic experimental details

Gas phase selective photo-oxidation tests were carried out with toluene and using a set-up described elsewhere [55]. Activity and selectivity for the gas-phase photooxidation were tested in a continuous flow annular photoreactor containing ca. 40 mg of photocatalyst as a thin layer coating on a pyrex tube. The corresponding amount of catalyst was suspended in 1 ml of ethanol, painted on a pyrex tube (cut off at ca. 290 nm) and dried at RT. The reacting mixture (100 ml/min) was prepared by injecting styrene

(≥99%; Aldrich) into a wet (ca. 75% relative humidity, RH) 20 vol.% O_2/N_2 flow before entering to the photoreactor, yielding an organic inlet concentration of ca. 700 ppmv. Under such conditions, the reaction rate shows a zero order kinetics with respect to the total flow and organic pollutant/oxygen concentrations. After flowing the mixture for 6 h (control test) in the dark, the catalyst was irradiated by four fluorescent daylight lamps (6W, Sylvania F6W/D) with a radiation spectrum simulating sunlight (UV content of 3%; main emission lines at 410, 440, 540, and 580 nm), symmetrically positioned outside the photoreactor. Similar tests were carried out in selected samples using UV lamps (Sylvania F6WBLT-65; 6W, maximum at ca. 350 nm). Reaction rates were evaluated under steady state conditions, typically achieved after ca. 8–10 h from the irradiation outset. No change in activity was detected for all samples within the next 10 h. The concentration of reactants and products was analyzed using an on-line gas chromatograph (Agilent GC 6890) equipped with HP-PLOT-Q/HP-Innowax columns (0.5/0.32 mm I.D. × 30 m) and TCD (for CO_2 measurement)/FID (organic measurement) detectors. Carbon balance was achieved in the 96–100% range in all experiments.

The quantum efficiency (Q.E.) for the reaction under UV and sunlight-type lights has been determined as the ratio between the number of molecules reacting by the number of photons interacting with the catalyst [56]:

$$\text{Q.E.\%} = \frac{\text{rate(mol m}^{-2}\ \text{s}^{-1})}{\text{photon rate(Einstein m}^{-2}\ \text{s}^{-1})} \times 100 \quad (1)$$

To evaluate the denominator of Eq. (1), we first evaluate the local net superficial rate of photon absorption, $e^{a,s}$, of the samples. The mathematical expression and modeling of the present sample-reactor system allowing such calculation is presented in the supplementary information.

3. Results and discussion

As mentioned in the Section 1, the control of the bismuth oxide polymorphism is critical in the context of its application in photocatalysis [31]. To analyze the phase behavior of the Bi precursor obtained by microemulsion, here we present an in situ XRD study of the pure Bi material evolution during calcination (Fig. 1). The precursor displays an XRD pattern ascribable to the bismuth subcarbonate phase, $Bi_2O_2CO_3$ (JCPDS card 41.1488; corresponding to the *I4/mmm* space group). Under treatment and at 300 °C this phase starts to evolve. Fig. 1B shows the key temperature region for such transformation; from 325 °C the carbonate phase is transformed into β-Bi_2O_3 (JCPDS card 74-1374; corresponding to the P-42$_1$c). The phase transformation appears complete at 425 °C. The region of stability of the beta phase is however rather limited; at 475 °C we already detected the γ-Bi_2O_3 phase (JCPDS card 45-1344; corresponding to the I23 space group). This phase is stable up to 750 °C; the end of the experiment. The thermal evolution presented in Fig. 1 is in agreement with previous results concerning the bismuth subcarbonate to oxide phase transformation in air [57]. The experiment highlights the fact that to obtain the beta polymorph (as a single or dominant phase) our materials must be calcined between 425 and 475 °C. Here we used 450 °C. The main chemical and morphological properties of the catalysts obtained after calcinations are summarized in Table 1. Except for the pure beta bismuth oxide, the preparation renders high surface are materials. The Bi–Ti composite system presents higher surface area than the two reference oxides; this indicates (see below) a modification of the titania morphology (primary particle size as well as particle–particle grain boundaries) and/or the presence of a Bi-containing high surface area component. The latter, according to the single Bi reference seems less likely, although this contribution should be small because of the low Bi_2O_3 content.

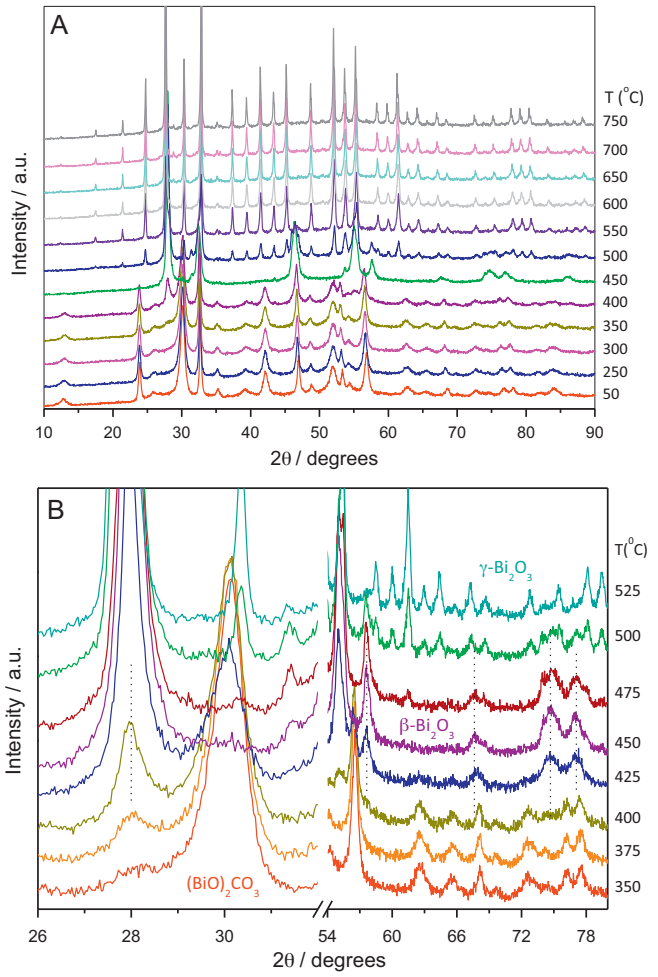

Fig. 1. XRD data of the Bi reference material during calcination. (A) General view; (B) detail view in the 350–525 °C range. Vertical lines in (B) mark β-Bi_2O_3 peaks easily discernible from other phases.

XRD patterns of the catalysts (Fig. 2) only present a contribution ascribable to the anatase structure (JCPDS card 78-2486, corresponding to the *I4$_1$/amd* space group). XRD analysis of the Ti reference and *x*BiTi composite catalysts shows that the anatase phase has a roughly constant particle size of ca. 9.9 ± 0.3 nm for samples with bismuth content up to 5 wt.%. Above that point the anatase particle size decreases markedly. Table 1 indicates that bismuth presence up to 5 wt.% triggers an increase of ca. 30 $m^2\ g^{-1}$. Because: (i) the surface area does not grow in parallel to the Bi content in the two 2.5BiTi and 5BiTi samples; (ii) the surface area of the Bi single reference seems not high enough to contribute; we can conclude that (iii) a modification of anatase morphology (more likely, anatase particle–particle network due to corresponding size constancy) occurs in the presence of Bi for catalysts with a Bi content below 5 wt. 5%. Further increase of surface area is observed

Table 1
Chemical and morphological properties for the *x*BiTi and reference samples.

Sample	Bi (wt.%)	S_{BET} ($m^2\ g^{-1}$)
Ti	0	84.3
2.5BiTi	2.8	113.6
5BiTi	5.2	112.4
10BiTi	10.6	136.1
Bi	100	13.6

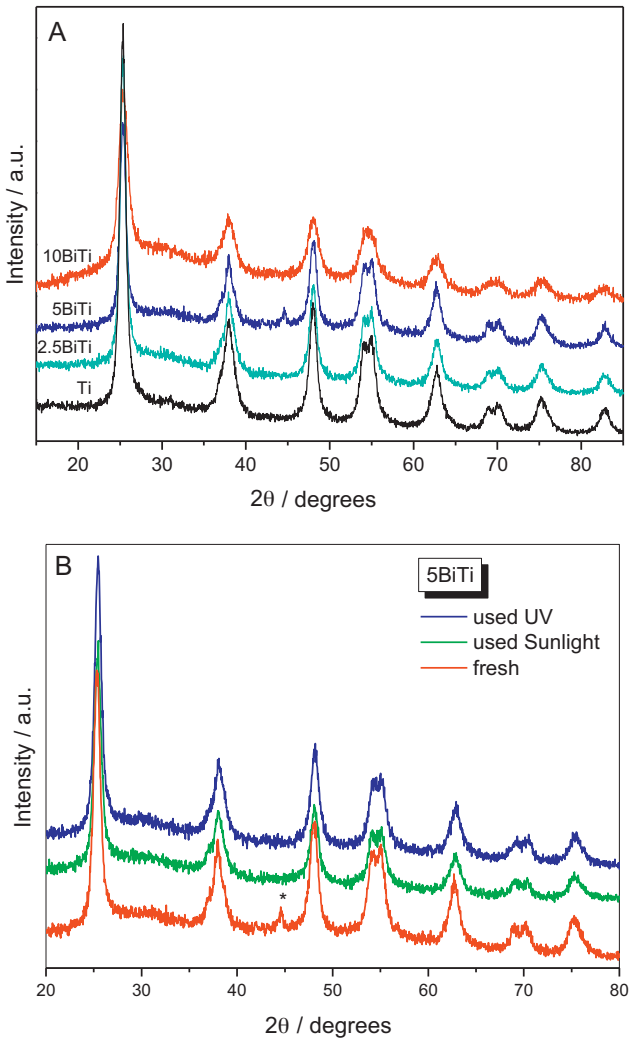

Fig. 2. XRD patterns for Ti reference and *x*BiTi samples: (A) fresh samples; (B) example of used samples. The asterisk marks a contribution from the sample holder.

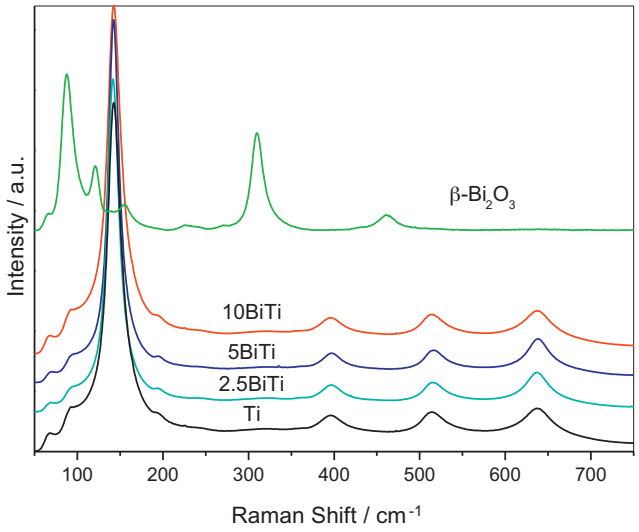

Fig. 3. Raman spectra for reference and *x*BiTi samples.

for the 10BiTi sample (with respect to other composite samples with lower Bi content – see Table 1). Thus, above 5 Bi wt.%, anatase primary particle size decreases concomitantly to the surface area increase detected from the 5BiTi sample.

The anatase phase is stable under reaction conditions. This issue was checked using XRD (see, as an example, Fig. 2B) and Raman (Fig. 3) of the postreaction, used samples. Table 2 summarizes the XRD analysis of anatase primary particle size which appears roughly invariant (within experimental error) under reaction conditions. Similarly to diffraction, Raman only detects the presence of the anatase phase with contributions at ca. 144, 195, 399, 517 and 639 cm^{-1} [50,58]. The constant position of anatase-related XRD and Raman peaks is strongly indicative of the absence of doping of the anatase component [4,45,59]. Another important point raised by the XRD/Raman techniques is the lack of identifiable signals coming from the bismuth component (compare the *x*BiTi sample outputs with the corresponding beta Bi_2O_3 pattern/spectrum in Figs. 1B and 3). This is not an uncommon situation in Bi–Ti composite samples [41,47]. As detailed below, this comes, at least partially, by the fact that bismuth alters anatase photochemistry from relatively low loadings [38–47], a fact complicating the detection and analysis of the component.

Table 2
Structural and optical properties for the *x*BiTi and reference samples.

Sample	Fresh/used XRD anatase particle size/nm	Band gap/eV	
		Fresh	Used UV/sunlight
Ti	9.6/9.7	3.03	2.97/2.96
2.5BiTi	10.6/10.5	3.01	2.95/3.00
5BiTi	9.6/9.5	3.10	3.05/3.07
10BiTi	6.2/6.0	2.96	2.93/3.01
Bi	–	2.39	–/–

In this work we carried out a XPS analysis of the samples to provide information related to the bismuth and, less importantly, titanium components of the composite samples. Absence of differences can be noticed for the Ti $2p_{3/2}$ XPS peak, which was observed at 458.6 ± 0.3 eV for all *x*BiTi composite and Ti reference samples. We however observed differences concerning the Bi component. Fig. 4 displays the Bi 4f region and, more concretely, the Bi $4f_{7/2}$ and $4f_{5/2}$ contributions. The former appears at 158.4/158.7 (2.5BiTi), 158.4/158.6 (5BiTi), 158.7/159.0 (10BiTi), and 158.6 (beta Bi_2O_3) eV for, respectively fast and slow (the latter to improve the S/N ratio to values usually reported, e.g. below 0.01–0.02, depending on Bi loading) scanning conditions. The binding energy values associated with the Bi $4f_{7/2}$ peak are all below 159.0 eV, characteristic of Bi(III) in an oxide chemical state [31,32,60,61]. Values above the 159.0 eV cut off can be also ascribed to carbonate phases [62], supporting in such cases a less clear assignment of the Bi local environment chemical nature. The *x*BiTi composite samples show (initial) binding energy values reasonably close to the reference (beta Bi_2O_3 158.6 eV; *x*BiTi samples within ±0.2 eV) and, as mentioned, all below 159.0 eV, indicating the similar chemical environment of Bi in composite and reference samples. A difference with the beta single oxide reference is, however, that the *x*BiTi samples evolve under X-ray excitation, showing a second, minor contribution at 156.6/156.9 eV. This is attributable to reduced Bi oxide phases or, more likely, to zerovalent Bi [60,63]. The existence of several oxygen deficient oxide phases of Bi^{3+} has already been reported [64]. The reduction of the Bi phase in contact with titania can be triggered by the small particle size of the Bi oxide nanoparticles and/or the interaction with anatase. As far as we know, X-ray induced reduction is not observed in the single Bi oxide phases [31,32]. Accordingly, such reduction effect is not detected in our beta Bi oxide reference but it seems a common issue for all *x*BiTi samples which, apparently, provides a route for a deep reduction of the initial oxidized Bi phase. For all these reasons it could thus

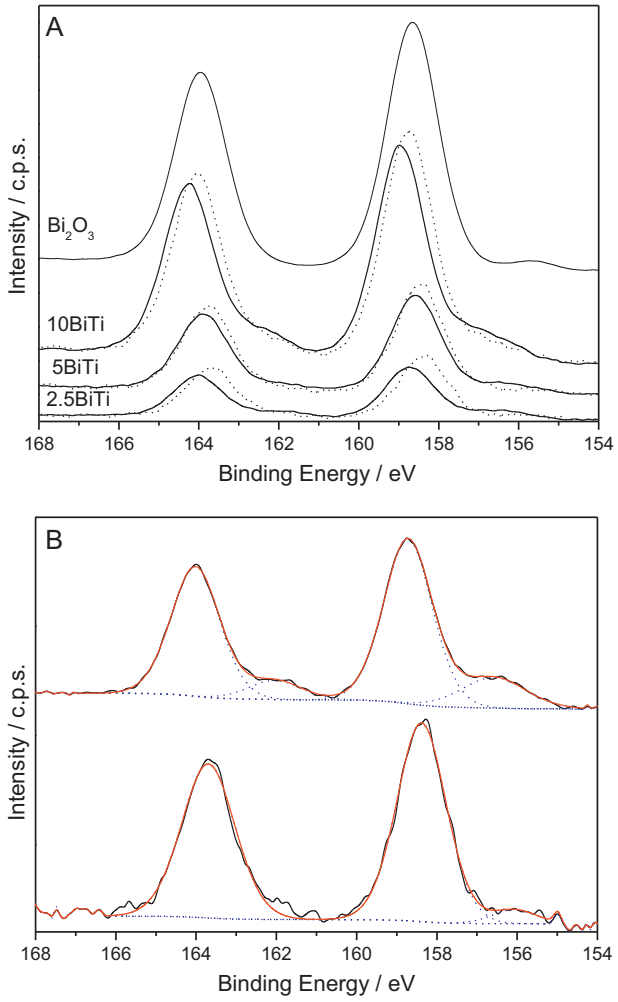

Fig. 4. Bi 4f spectra for (A) the *x*BiTi samples and the beta Bi single oxide reference; (B) detail of fitting for the 2.5BiTi sample. In A two spectra are presented for each sample concerning fast (dashed line) and normal (full line) scanning conditions. The Bi reference intensity is divided by 15 to scale. In (B) the experimental spectra (full line; black) are presented with fitting results (dashed line; in blue we plot all components used and in red the corresponding envelope curve). (For interpretation of the references to color in text, the reader is referred to the web version of this article.)

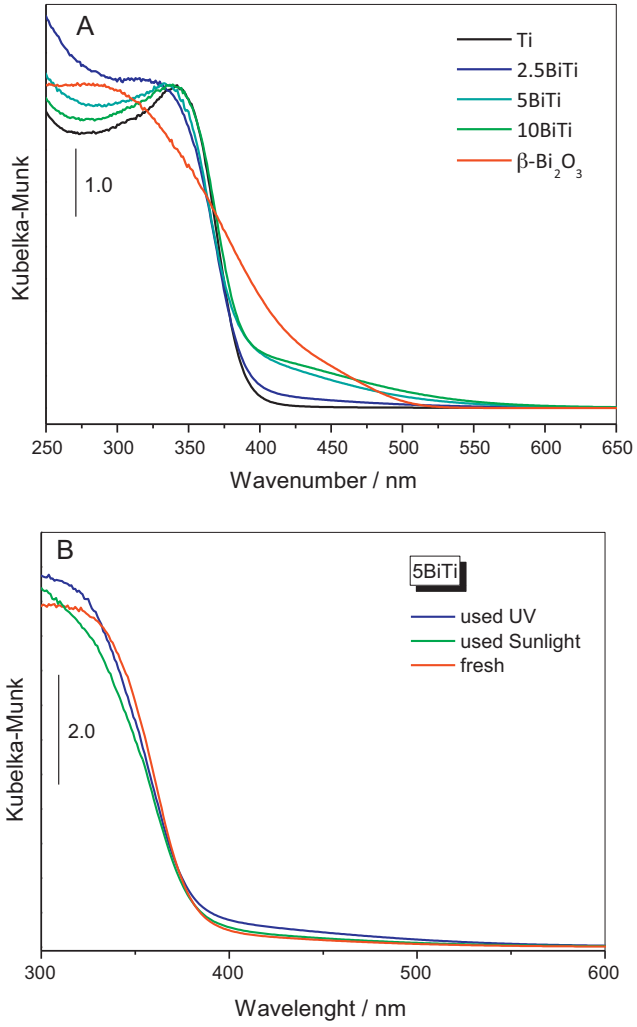

Fig. 5. UV–vis spectra of reference and *x*BiTi samples: (A) fresh samples; (B) example of used samples.

be ascribed to an electronic effect of the titania phase, influencing the reducibility of the Bi component. In our samples, this effect is probably promoted by a large interaction surface between the two (Bi and Ti) components. Therefore, this would be a fingerprint of the electronic contact or interaction between the two oxides.

Optical properties and particularly photon absorption are of capital importance to interpret photo-catalytic behavior. Fig. 5 displays the UV–vis spectra of the reference and composite catalyst. The Bi–Ti composite samples present a main feature dominated by the anatase band gap. As expected from the chemical compositions displayed in Table 1, the band gap energy (calculated considering the material an indirect gap semiconductor, as anatase) shows an almost constant value for all composite samples. As presented in Table 2, such value is equal to the titania reference roughly within experimental error (±0.05 eV). This is consistent with the previous characterization results which indicate the absence of doping or mayor structural effects in the anatase phase. The beta bismuth oxide reference presents a lower (than anatase) bang gap of ca. 2.4 eV, previously observed for this polymorph [31,34]. Although the Bi–Ti composite systems do not show significant differences in the gap energy, Fig. 5 evidences some differences in the 400–550 nm region. The comparison with the bismuth reference material indicates that the corresponding electronic states are related to such component and grow with the Bi content of the catalyst. This optical contribution is obviously responsible for allowing the use of the visible part of the electromagnetic spectrum. The UV–vis spectra of the Bi–Ti composite systems do not display appreciable modification after reaction; Fig. 5B provides a representative example.

The activity of the samples for the degradation of toluene under UV and sunlight-type excitations is shown in Fig. 6. At the supplementary information section we present a representative example of the BiTi composite photocatalytic behavior under the prolonged reaction test used here. A pseudo-steady state is reached in all cases and Fig. 6 displays result after ca. 20 h on stream, indicating the reasonable stability of the materials. In Fig. 6 the first thing to note is that nanometric anatase (Ti reference) is a relatively active material for toluene degradation, showing in our specific case (sample by microemulsión and calcined at 450 °C) higher activity than the P25 reference material [6,7,49], while the Bi reference here tested is not, despite being the beta polymorph. The low activity of the beta Bi_2O_3 phase for toluene degradation is nevertheless a somewhat expected result due to the tough test that such reaction is; for example, other (than anatase) photocatalytic oxides like WO_3 or CeO_2 did not show appreciable activity if compared with nano-anatase [49,65,66]. For the *x*BiTi samples, a different behavior is observed

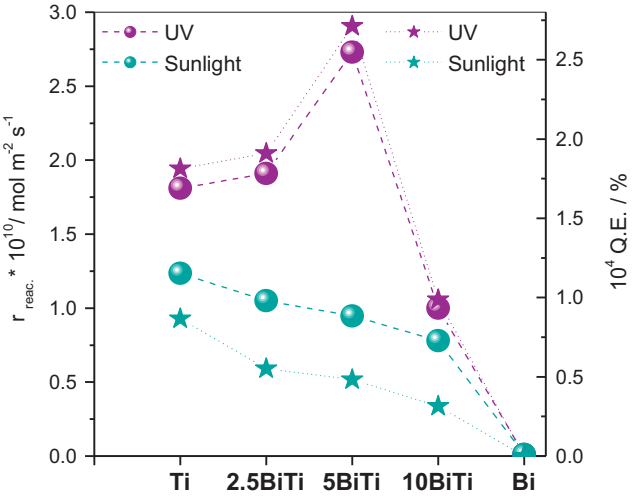

Fig. 6. Reaction rates and quantum efficiency for reference and *x*BiTi samples.

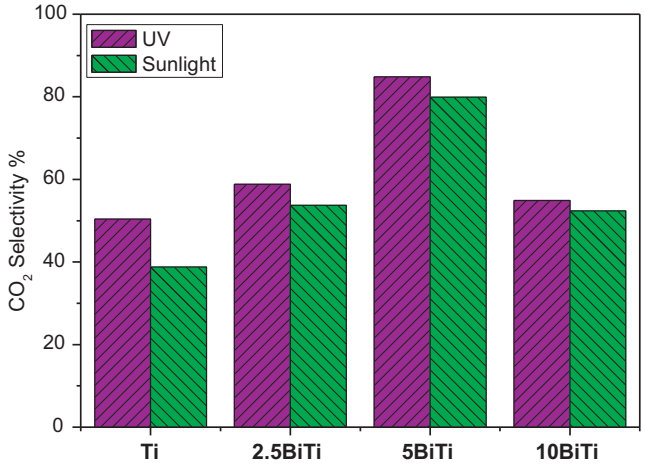

Fig. 7. Selectivity to CO_2 for reference and *x*BiTi samples.

along the series under UV and sunlight. Under UV Fig. 6 shows an increase of the normalized (by surface area) reaction rate up to the 5BiTi samples with subsequent decrease after it. The 10BiTi sample performs worse than the Ti reference sample. A more quantitative analysis was obtained by calculating the quantum efficiency parameter. Using this parameter, the behavior under UV light is similar to the reaction rate. In the case of sunlight, the quantum efficiency is nearly constant for all the *x*BiTi composite samples, with a weak maximum for the 2.5BiTi sample. The *x*BiTi sunlight-type quantum efficiency values are however below the corresponding of the Ti reference. So, in the *x*BiTi samples we observed a strong increase of activity of ca. 2.2 under UV light and a limited activity upon sunlight. This last factor is more clearly detected using the efficiency parameter rather than the reaction rate.

The Bi–Ti series behavior is in relative opposition to the general, net enhancement observed for Bi–Ti composite samples upon light excitation above 420 nm, for other, possibly less demanding, test reactions [38–47]. We however agree with all previous works in the fact that the most active composite sample contains a Bi amount always below 10 wt.%. Due to the relatively limited information concerning structural details of the Bi phase at atomic level in the composite system, a issue shared by this study and all previously published reports [38–47], it is difficult to discussed further this point but details of the oxide environment of Bi seems likely in the origin of the differences among the *x*BiTi samples. This line of reasoning can be justified in the large activity differences detected among the pure Bi_2O_3 phases [31], which may be thus a contributing factor in the composite case even if the structural differences are of lower magnitude than those concerning the pure polymorphs of the Bi oxide phase. In the composite photocatalysts, the structural differences may be directly related to an effect of titania, as the XPS results suggest. We would also like to note that, assuming a constant structural interaction situation, the contact of Bi and Ti oxide phases seems only weakly size-dependent in the nanometer range [4]. Thus Bi particle size in the nanometer range (well below ca. 5 nm) per se would be a secondary factor to justify the observed differences among our *x*BiTi composite photocatalysts. A final point to mention is the progressive modification of the particle size of anatase as well as particle–particle networking modification observed in the presence of bismuth (Tables 1 and 2). In the case of toluene photo-oxidation, the decrease of particle size from ca. 10 nm (pure and low Bi loading) to ca. 6 nm (10BiTi sample) has been shown detrimental for activity [4,67,68]. This is commonly discussed in terms of the broad term of crystallinity of the anatase nanomaterial. As quantum size effects in anatase band gap are absent in our sample series (Table 2), the titania morphology effect on photo-activity seems here related to defect and surface structure and their relationship with anatase photo-chemistry [4].

The presence of Bi in the *x*BiTi composite samples also influences other photocatalytic parameters such as the selectivity. As occurs for the nano-titania reference system [6,7], toluene photo-oxidation only produces benzaldehyde as detectable partial oxidation product and CO_2 as the total oxidation one. The plot presented in Fig. 7 indicates however an important modification of the selectivity in the presence of Bi, with a maximum to the total oxidation product for the 5BiTi sample. In no case, the selectivity to CO_2 presented by the titania reference is degraded by the presence of Bi; this occurring both upon UV and sunlight-type excitation. Such an effect is therefore another beneficial effect of the Bi presence in the composite photocatalysts, which appears independent of the excitation wavelength and accounts for a maximum enhancement of ca. 30–35%. The general, enhanced selectivity to the total oxidation pathway can be an effect of a better hole availability (the active species in toluene photo-oxidation; see Refs. [69–71]) to generate chemistry. This can be originated from an improved charge handling occurring by a combination of two effects related to the active titania phase: the contact with a Bi oxide phase as well as the anatase morphology modification along the BiTi series [4]. The effect of the Bi–Ti interaction in charge separation after excitation has been previously claimed in all previous reports concerning the Bi–Ti system [38–47]. Such combined effect could justify the enhanced photocatalytic properties, activity and selectivity, presented in the Bi–Ti binary system with respect to the Ti reference material.

4. Conclusions

A series of three Bi_2O_3–TiO_2 composite catalysts, with bismuth loading in the 2–5–10 wt.% range, were prepared by microemulsion using a single pot procedure followed by calcinations at 450 °C. A multitechnique XRD–XPS–Raman–UV–vis study of the materials was used to characterize the catalysts. The presence of bismuth in an oxide environment is demonstrated for all composite samples. In parallel, the growth of the bismuth content modifies the anatase morphology, yielding a decrease of the anatase particle size from the 5BiTi sample. The latter occurs without significant modification of the optical properties of the anatase phase according to the UV–vis spectroscopy.

Composite samples improve the performance of TiO_2 by a maximum factor of 2.2 (UV case) and increase significantly the selectivity to the total oxidation product, CO_2, upon both UV and sunlight

excitation conditions. Optimum performance in terms of activity and selectivity was achieved with the 5BiTi sample and appears as a combination of two factors related (in either an indirect or direct way) to the anatase active phase. The first is connected to the contact between the two oxides, a fact which is (indirectly) suggested by XPS through the easy reduction of the bismuth phase. The presence of a Bi oxide phase in contact with anatase is known to affect the charge handling properties after light excitation. The second is the morphology modification of the anatase component, which displays a decreased particle size for loadings of bismuth above 5 wt.%. The particle size decrease from ca. 10 nm is also known to be detrimental for toluene photo-oxidation. Both effects seem to affect the photo-chemistry of the composite materials in toluene degradation with respect to the two single oxide reference systems, and explain the optimum performance displayed by the 5BiTi sample as a compromise between these two effects.

Acknowledgements

M.N. Gómez-Cerezo would like to acknowledge the Universidad Autónoma de Madrid for a Master Thesis Grant. A. Kubacka and M. J. Muñoz-Batista thank Ministerio de Economía y Competitividad (MINECO) for support thought, respectively, the postdoctoral "Ramón y Cajal" and predoctoral FPI programs. Financial support by MINECO is also acknowledged (project CTQ2010-14872/BQU).

Appendix A. Supplementary data

Supplementary data associated with this article can be found, in the online version, at http://dx.doi.org/10.1016/j.apcatb.2014.03.024.

References

[1] M.R. Hoffman, S.T. Martin, W. Choi, D.W. Bahneman, Chem. Rev. 95 (1995) 69–121.
[2] O. Carp, C.L. Huisan, A. Reller, Prog. Solid State Chem. 32 (2004) 33–145.
[3] H. Thu, M. Karkmaz, E. Puzenat, C. Guillard, J.M. Herrmann, Res. Chem. Intermed. 31 (2005) 449–543.
[4] A. Kubacka, G. Colón, M. Fernández-García, Chem. Rev. 112 (2012) 1555–1614.
[5] M. Anpo, M. Takeuchi, J. Catal. 216 (2003) 505–516.
[6] A. Kubacka, M. Fernández-García, G. Colón, J. Catal. 254 (2008) 272–281.
[7] A. Kubacka, G. Colón, M. Fernández-García, Catal. Today 143 (2009) 286–292.
[8] M. Khan, Y. Song, N. Chen, W. Cao, Mater. Chem. Phys. 142 (2013) 148–153.
[9] R. Asahi, T. Morikawa, T. Ohwaki, K. Aoki, Y. Taga, Science 293 (2001) 269–277.
[10] N. Serpone, J. Phys. Chem. B 110 (2006) 24287–24331.
[11] C. Belver, R. Bellod, S.J. Stewart, F.G. Requejo, M. Fernández-García, Appl. Catal. B 65 (2006) 309–314.
[12] A. Kubacka, B. Bachiller-Baeza, B.G. Colón, M. Fernández-García, J. Phys. Chem. C 113 (2009) 8553–8556.
[13] A. Kubacka, B. Bachiller-Baeza, G. Colón, M. Fernández-García, Appl. Catal. B 93 (2010) 274–281.
[14] A. Kubacka, G. Colón, M. Fernández-García, Appl. Catal. B 95 (2010) 238–244.
[15] H. Gao, B. Lu, F. Liu, X. Shao, Int. J. Photoenergy (2012), ID 453018.
[16] C.W. Lai, S. Sreekantan, J. Alloys Compd. 547 (2013) 43–50.
[17] J. Gou, et al., J. Appl. Phys. 114 (2013) 104803.
[18] D. Robert, Catal. Today 122 (2007) 20–33.
[19] A.M. Balu, B. Baruwati, E. Serrano, J. Cot, J. García-Martínez, R.S. Varma, R. Luque, Green Chem. 13 (2011) 2750–2758.
[20] V. Augugliaro, L. Yurdakal, V. Loddo, G. Palmisano, L. Palmisano, Adv. Chem. Eng. 20 (2009) 1–35.
[21] G. Colón, S. Murcia López, M.C. Hidalgo, J.A. Navío, Chem. Commun. (2010) 4809–4811.
[22] M.J. Kim, K-.D. Kim, H.-D. Seo, Y. Luo, N.K. Dey, Y.D. Kim, Appl. Surf. Sci. 258 (2011) 2489–2499.
[23] N.K. Dey, M.J. Kim, K.-D. Kim, K.H. Lee, J. Mol. Catal. A 337 (2011) 33–38.
[24] R.G. Nair, J.K. Roy, S.K. Samdarshi, A.K. Mukherjee, Solar Energy Mater. Solar Cells 105 (2012) 103–108.
[25] J. Tokarsky, V. Tatejka, L. Neuwirthova, J. Vontorova, J. Mamulova, K. Kutlakova, J. Kukutschova, P. Capkova, Chem. Eng. J 222 (2013) 488–497.
[26] P.V. Kamat, J. Phys. Chem. C 111 (2007) 2834–2867.
[27] M.C. Hidalgo, M. Maicu, J.A. Navío, G. Colón, J. Phys. Chem. C 113 (2009) 12840–12846.
[28] M. Taylor, E.N. Ndifor, T. Garcia, B. Solsona, A.F. Carley, S.H. Taylor, Appl. Catal. A 350 (2008) 63–70.
[29] R.G. Nair, A.M. Tripathi, S.K. Samdarshi, Energy 36 (2011) 3342–3347.
[30] Z. Wen, W. Wu, Z. Liu, H. Zheng, J. Li, J. Chen, Phys. Chem. Chem. Phys. 15 (2013) 6773–6778.
[31] H. Chen, B. Huang, J. Lu, Z. Wang, B. Xu, X. Quin, X. Zhang, Y. Dai, Phys. Chem. Chem. Phys. 12 (2010) 15468–15475.
[32] J.K. Reddy, B. Srinivas, V.D. Kumari, M. Subrahmanyam, ChemCatChem 1 (2009) 492–499.
[33] H. Zhang, P. Wu, Y. Li, L.F. Liao, Z. Fang, X.H. Zhong, ChemCatChem 2 (2010) 1115–1121.
[34] K. Brezesinski, R. Ostermann, P. Hartmann, J. Parlich, T. Brezesinski, Chem. Mater. 22 (2010) 3079–3085.
[35] J. Hou, C. Yang, W. Zhou, S. Jiao, H. Zhu, Appl. Catal. B 142–143 (2013) 504–511.
[36] A. Hameed, V. Gombac, T. Montini, M. Graziani, P. Fornasiero, Chem. Phys. Lett. 472 (2009) 212–216.
[37] A. Hameed, V. Gombac, T. Montini, L. Felisari, P. Fornasiero, Chem. Phys. Lett. 472 (2009) 254–261.
[38] J. Xu, Y. Ao, D. Fu, C. Yuan, Appl. Surf. Sci. 255 (2008) 2365–2369.
[39] L. Lin, J. Wang, Y. Qu, Y. Luan, Appl. Surf. Sci. 256 (2009) 657–663.
[40] S. Shamaila, A.K.L. Sajjad, F. Chen, J. Zhang, Appl. Catal. B 94 (2010) 272–280.
[41] J. Hou, C. Yang, Z. Wang, S. Jiao, H. Zhu, Appl. Catal. B 129 (2013) 333–341.
[42] Y. Huo, X. Chen, J. Zhang, G. Ran, J. Jia, H. Li, Appl. Catal. B 148–149 (2013) 550–556.
[43] Z. Bian, J. Zhu, S. Wang, Y. Cao, X. Quian, H. Li, J. Phys. Chem. C 112 (2008) 6258–6262.
[44] J. Zhu, S. Wang, J. Wang, D. Zhang, H. Li, Appl. Catal. B 102 (2011) 120–125.
[45] K. Su, Z. Ai, L. Zhang, J. Phys. Chem. C 116 (2012) 17118–17123.
[46] D. Li, Y. Zhang, X. Zhou, S. Gou, J. Hazard. Mater. 258–259 (2013) 42–49.
[47] J. Yuang, J. Dan, J. Li, Environ. Sci. Pollut. Res. 20 (2013) 2435–2447.
[48] P.G. De Gennes, C. Taupin, J. Phys. Chem. 86 (1982) 2294–2303.
[49] A. Fuerte, M.D. Hernández-Alonso, A.J. Maira, A. Martínez-Arias, M. Fernández-García, J.C. Conesa, J. Soria, G. Munuera, Chem. Commun. (2001) 2718–2719.
[50] M. Fernández-García, X. Wang, C. Belver, J.C. Hanson, J.A. Rodriguez, J. Phys. Chem. C 111 (2007) 674–682.
[51] C. Greaves, S.K. Blower, Mater. Res. Bull. 23 (1988) 1001–1007.
[52] A. Le Bail, H. Duroy, J.L. Forquet, Mater. Res. Bull. 23 (1988) 447–453.
[53] G.K. Williamson, W.H. Hall, Acta Metall. 1 (1953) 22–31.
[54] J. Tauc, Mater. Res. Bull. 5 (1970) 721–729.
[55] M.J. Muñoz-Batista, A. Kubacka, M.N. Gómez-Cerezo, D. Tudela, M. Fernández-García, Appl. Catal. B 140–141 (2013) 626–635.
[56] B. Ohtani, Chem. Lett. 37 (2008) 167–189.
[57] H.F. Cheng, B.B. Huang, K.S. Yang, Z.Y. Wang, X.Y. Quin, X.Y. Zhang, Y. Dai, ChemPhysChem 11 (2010) 2167–2176.
[58] M. Mikami, S. Nakamura, O. Kitao, H. Arakawa, Phys. Rev. B 66 (2002) 155213–155216.
[59] Z. Bian, J. Ren, J. Zhu, S. Wang, Y. Lu, H. Li, Appl. Catal. B 89 (2009) 577–582.
[60] C.D. Wagner, W.M. Riggs, L.E. Davis, J.F. Moulder, in: G.E. Muilenberg (Ed.), Handbook of X-Ray Photoelectron Spectroscopy, Perkin-Elmer, Minesota, 1978.
[61] K. Uchida, A. Ayame, Surf. Sci. 357 (1996) 170–178.
[62] Q. Li, H. Liu, F. Dong, M. Fu, J. Colloid Interface Sci. 408 (2013), 33.42.
[63] P.S.A. Kumar, S. Muhamuni, A.S. Nigavekar, S.K. Kulkarni, Physica C 201 (1992) 145–151.
[64] A. Hameed, T. Montini, V. Gombac, P. Fornasiero, J. Am. Chem. Soc. 130 (2008) 9658–9659.
[65] M.D. Hernández-Alonso, A.B. Hungría, A. Martínez-Arias, J.M. Coronado, J.C. Conesa, J. Soria, M. Fernández-García, Phys. Chem. Chem. Phys. 6 (2004) 3524–3529.
[66] M.D. Hernández-Alonso, A.B. Hungría, A. Martínez-Arias, M. Fernández-García, J.M. Coronado, J.C. Conesa, J. Soria, Appl. Catal. B 50 (2004) 167–175.
[67] R. Khan, S.W. Kim, T.-J. Kim, H. Lee, Bull. Korean Chem. Soc. 28 (2007) 1951–1957.
[68] M. Inagaki, R. Nonaka, B. Tryba, A.W. Morawski, Chemosphere 64 (2006) 437–445.
[69] M. Sleiman, P. Conchon, C. Ferronato, J.-M. Chovelon, Appl. Catal. B 86 (2009) 159–165.
[70] J. Mo, Y. Zhang, A. Xu, Y. Zhu, J.J. Lamson, R. Zhao, Appl. Catal. B 89 (2009) 570–576.
[71] M. Muñoz-Batista, M.N. Gómez-Cerezo, A. Kubacka, D. Tudela, M. Fernández-García, ACS Catal. 4 (2014) 63–72.